Polymeric Vesicles

Deutsche Ausgabe: DOI: 10.1002/ange.201509401
Internationale Ausgabe: DOI: 10.1002/anie.201509401

Enzyme-Responsive Polymeric Vesicles for Bacterial-Strain-Selective Delivery of Antimicrobial Agents

*Yamin Li, Guhuan Liu, Xiaorui Wang, Jinming Hu, and Shiyong Liu**

Abstract: *Antimicrobial resistance poses serious public health concerns and antibiotic misuse/abuse further complicates the situation; thus, it remains a considerable challenge to optimize/improve the usage of currently available drugs. We report a general strategy to construct a bacterial strain-selective delivery system for antibiotics based on responsive polymeric vesicles. In response to enzymes including penicillin G amidase (PGA) and β-lactamase (Bla), which are closely associated with drug-resistant bacterial strains, antibiotic-loaded polymeric vesicles undergo self-immolative structural rearrangement and morphological transitions, leading to sustained release of antibiotics. Enhanced stability, reduced side effects, and bacterial strain-selective drug release were achieved. Considering that Bla is the main cause of bacterial resistance to β-lactam antibiotic drugs, as a further validation, we demonstrate methicillin-resistant S. aureus (MRSA)-triggered release of antibiotics from Bla-degradable polymeric vesicles, in vitro inhibition of MRSA growth, and enhanced wound healing in an in vivo murine model.*

Since their commercial introduction in 1940s, antibiotics have substantially reduced human morbidity and mortality. Unfortunately, pathogens can develop antibiotic resistance through de novo gene mutation or horizontal gene transfer. Furthermore, antibiotic abuse/misuse has produced more virulent and resistant strains, which pose huge threats to global health.[1] Therefore, it is necessary to screen for next-generation antibiotics and explore therapeutically effective strategies. The invention of antibiotics by high-throughput screening of natural products and chemical libraries was successful before 1970s, but the progress has been extremely slow since then. On the other hand, nanoparticle-based drug delivery strategies aiming to improve therapeutic efficacy of currently available antibiotics provides an alternate solution.[2]

Among various inorganic and polymeric drug nanocarriers, polymeric vesicles self-assembled from amphiphilic block copolymers can encapsulate both hydrophobic and hydrophilic payloads ranging from low to ultrahigh molecular weight species (such as antibiotics, therapeutic peptides/proteins, and bacteriophage).[3] Stimuli-responsive polymeric vesicles with tunable permeability possessing a "sense and act" module for on-demand drug release in a spatiotemporal and dosage-controlled manner are highly advantageous for antibiotic delivery.[4] As for triggering motifs, enzymes provide the most promising ones as enzymatic reactions are highly selective and efficient under mild conditions, and involved in all biological, metabolic, and pathological processes.[5] Most importantly, specific enzymes are actively produced by resistant pathogens (for example, penicillin G amidase (*PGA*) and β-lactamase (*Bla*)),[6] and *Bla*-catalyzed hydrolysis is mainly responsible for drug resistance towards a series of β-lactam antibiotic drugs, such as penicillin, cephalosporin, and carbapenem.

Note that enzyme-responsive polymeric vesicles have been far less explored.[7] The only two reports concerning bacterial enzyme-responsive polymeric vesicles focused on fluorescent bacteria detection under simulated conditions, and none of these enzymes are relevant to the acquisition of bacterial resistance.[7e,f] Herein, we aim to establish a general strategy to construct bacterial strain-selective delivery nanocarriers for antimicrobial agents based on block copolymer vesicles, which are responsive to enzymes relevant to clinically important bacterial strains (Scheme 1). *PGA* and *Bla*-responsive polymeric vesicles were self-assembled from amphiphilic diblock copolymers consisting of hydrophilic poly(ethylene glycol) (PEG) block and hydrophobic block containing enzyme-cleavable self-immolative side linkages. During vesicle formation, antimicrobial agents were loaded into either hydrophobic bilayers or aqueous interiors. Upon incubation with specific enzymes, the chemical structural transformation, morphology transition, drug release profile, and antibacterial activities of polymeric vesicles were investigated.

In previously reported systems concerning enzyme-responsive polymeric nanoparticles, an enzymatic backbone scission mechanism was solely involved.[7] However, the diversity in enzymes and substrates leads to drastically different degradation kinetics and release profiles. In this work, we attempted to introduce side chain enzymatic cleavage mechanism, and chose *PGA* and *Bla* as target enzymes, considering that both enzymes are associated with bacterial resistance. As shown in Scheme 1, side chain moieties in hydrophobic blocks of PEG-*b*-PP and PEG-*b*-PC are subjected to enzymatic uncapping of terminal groups (phenylacetic amide and cephalosporin) and subsequent self-immolative cleavage (spontaneous rearrangement through

[*] Y. Li, Dr. G. Liu, X. Wang, Dr. J. Hu, Prof. Dr. S. Liu
CAS Key Laboratory of Soft Matter Chemistry
Hefei National Laboratory for Physical Sciences at the Microscale
iChem (Collaborative Innovation Center of Chemistry for Energy Materials)
Department of Polymer Science and Engineering
University of Science and Technology of China
Hefei, Anhui Province 230026 (China)
E-mail: sliu@ustc.edu.cn

Supporting information, including experimental details, characterization methods, and all relevant characterization data, and ORCID(s) from the author(s) for this article are available on the WWW under http://dx.doi.org/10.1002/anie.201509401.

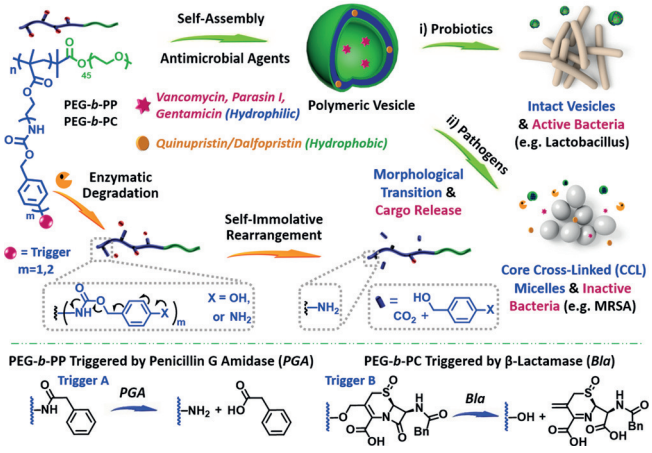

Scheme 1. Enzyme-responsive polymeric vesicles for bacterial strain-selective delivery of antibiotics. Polymeric vesicles self-assembled from PEG-*b*-PP and PEG-*b*-PC are subjected to side chain cleavage and microstructural transformation in response to penicillin G amidase (*PGA*), and β-lactamase (*Bla*), respectively. This process is accompanied with sustained release and bioactivity recovery of antimicrobial agents encapsulated within vesicles.

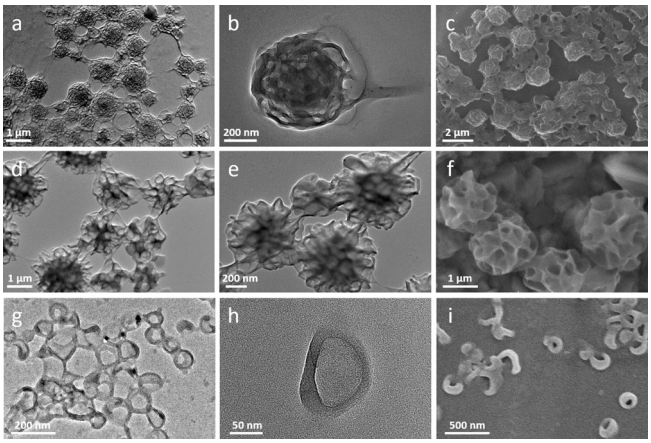

Figure 1. TEM (left and middle columns) and SEM (right column) images of: a–c), **PP2** LCVs; d–f), **PP4** LCVs; g–i), **PC1** vesicles.

1,6-elimination of *p*-hydroxybenzyl alcohol or *p*-aminobenzyl alcohol), both affording poly(2-aminoethyl methacrylate) scaffolds.[8] By involving side chain degradation triggered by drug-resistant enzymes and final nanostructures with comparable chemical compositions, we aim to achieve controlled degradation kinetics, predictable payload release profiles, and targeted antibiotic delivery.

PGA- and *Bla*-responsive monomers, **PBC** and **CBC**, were first synthesized (Supporting Information, Figures S1–S3). Reversible addition-fragmentation chain transfer (RAFT) polymerization of **PBC** using PEG_{45} macroRAFT agent (PEG_{45}-CTA) afforded *PGA*-responsive PEG-*b*-PP (**PP1**-**PP5**) diblock copolymers (Figures S4-S5 and Table S1). However, **CBC** cannot be polymerized under the same conditions, which was likely due to the relatively high steric hindrance. Alternatively, a polymerizable precursor bearing latent isocyanate functionality, **BBC**, was synthesized (Figures S1 and S6). RAFT polymerization of **BBC** using PEG_{45}-CTA afforded PEG-*b*-PB (**PB1**-**PB2**) (Figures S4 and S7). After reacting with **PHCC** and deprotection of ester linkages, *Bla*-responsive PEG-*b*-P(C-*co*-B) (**PC1**-**PC2**) block copolymers were obtained (Figures S4 and S8, Table S1). Polarity-sensitive probe, 3-hydroxyflavone (3-HF)-labeled and *PGA*-responsive **PP6** and enzyme-inert PEG-*b*-polystyrene (PEG-*b*-PS, **PS1**) were also synthesized (Figures S9 and S10a, Table S2).

Self-assembly of above diblock copolymers was conducted using the cosolvent approach. Assemblies with uniform morphologies, such as spherical micelles, vesicles, large compound vesicles (LCVs),[9a] and large compound micelles (LCMs), were obtained (see the Supporting Information).[9] These nanostructures were characterized by dynamic light scattering (DLS), transmission electron microscopy (TEM), scanning electron microscopy (SEM), and atomic force microscopy (AFM) (Figure 1; Supporting Information, Figures S11–S13). In spite of varying chemical structures/compositions and hydrophobic block lengths, the general trend of vesicles and LCVs formation (Table S1) can be ascribed to synergistic and cooperative effects from hydrophobic, hydrogen bonding, and π-π stacking interactions between carbamate-containing hydrophobic blocks.[8d]

Next, the colloidal stability of polymeric vesicles was examined by fluorescence and DLS measurements. In the absence of *PGA*, both fluorescence resonance energy transfer (FRET) ratios (I_{575}/I_{505}) of DiO/DiI co-loaded **PP2** LCVs and emission intensities of ESICT (excited state intramolecular charge transfer; 451 nm) and ESIPT (excited state intramolecular proton transfer; 537 nm) bands of 3-HF-labeled **PP6** LCVs exhibited negligible changes (Figures 2a; Supporting Information, Figure S14). The long-term stability of **PP2** LCVs and **PC1** vesicles were also confirmed by DLS (Figures 2b; Supporting Information, Figure S15a). Moreover, both hydrodynamic diameters ($\langle D_h \rangle$) and polydispersities (μ_2/Γ^2) of **PP2** LCVs showed no obvious changes when dispersed in PBS or 20% fetal bovine serum (FBS; Figure S15b).

The loading capability of polymeric vesicles was then examined by fluorescence measurements and confocal laser scanning microscopy (CLSM), using hydrophilic/hydrophobic small molecule dyes (calcein and Nile red (NR)) and fluorescent macromolecules (FITC-parasin I) as model payloads (Figure S16). Moreover, the concurrent loading of calcein/NR or FITC-Parasin I/NR was verified by CLSM technique (Figure 2f; Supporting Information, Figure S17). Encapsulating antibiotics and therapeutic proteins into polymeric vesicles is expected to enhance their structural stabilities, as bioactive molecules are often unstable when exposed to elevated temperature, ionic strengths, and enzymes. To confirm this, chlorophenol red-β-D-galactopyranoside (CPRG, as a small molecular antibiotic model) and myoglobin (Myo, as a therapeutic protein model) were loaded into **PP2** LCVs, respectively (Figure S18). Free CPRG can be readily cleaved by β-galactosidase to generate chlorophenol red (CPR), whereas no colorimetric reaction occurred when CPRG was encapsulated within **PP2** LCVs (Figure S19). Furthermore, although the protein activity of free Myo

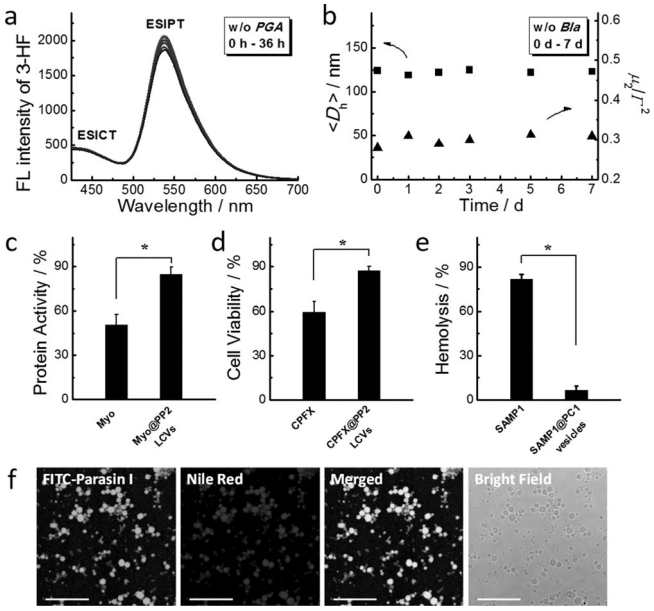

Figure 2. Time-dependent evolution of a) fluorescence emission spectra of DiO/DiI co-loaded **PP2** LCVs in the absence of *PGA*, and b) hydrodynamic diameters ($\langle D_h \rangle$) and polydispersities (μ_2/Γ^2) of **PC1** vesicles in the absence of *Bla*. c) Enhanced stability of myoglobin (Myo) encapsulated in **PP2** LCVs. d,e) Reduced side effects of CPFX-loaded **PP2** LCVs against HeLa cells and **SAMP1**-loaded **PC1** vesicles against human red blood cells. f) CLSM images of FITC-parasin I/NR co-loaded **PP2** LCVs (scale bars = 10 μm); $*p < 0.01$, student's *t*-test.

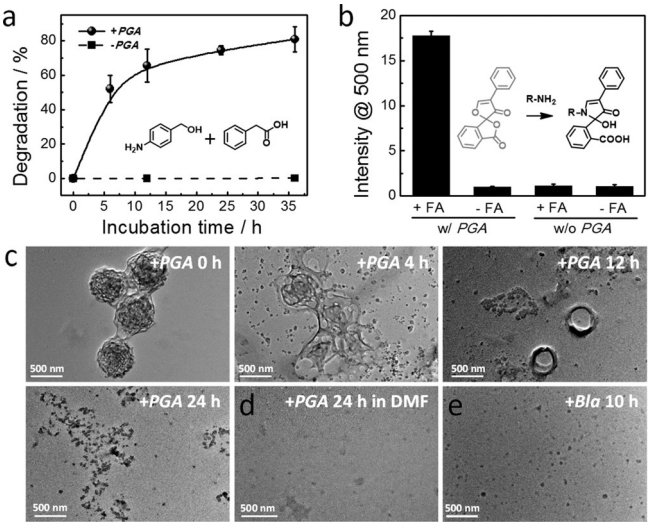

Figure 3. Enzyme-triggered degradation of polymeric vesicles. a) Percentage degradation of **PP2** LCVs against incubation duration in the absence and presence of *PGA*. b) Fluorescence analysis of **PP2** LCVs in the absence and presence of fluorescamine (FA) with or without *PGA* degradation. c) Time-dependent evolution of *PGA*-digested **PP2** LCVs. TEM images of d) *PGA*-treated **PP2** LCVs diluted with DMF and e) *Bla*-treated **PC1** vesicles.

gradually decayed within 2 days, **PP2** LCVs encapsulating Myo showed much less bioactivity loss, as verified by the guaiacol oxidation assay (Figure 2c).

On the other hand, antibiotics and macromolecular antimicrobial agents typically incur adverse effects (e.g. nephrotoxicity for vancomycin, cytotoxicity for ciprofloxacin (CPFX), and hemolysis for antimicrobial polymers). Loading of them within polymeric vesicles could attenuate side effects (Figure S20). Although free CPFX showed cytotoxicity against HeLa cells, **PP2** LCVs encapsulated CPFX exhibited negligible effects on cell viabilities (Figure 2d). Additionally, loading antimicrobial polymer **SAMP1** (Figure S9) into **PC1** vesicles could significantly reduce hemolysis against human red blood cells (hRBCs; Figure 2e).

The enzymatic degradation process was then studied. Upon *PGA* incubation, ≈80% of side chain moieties of **PP2** were digested within 36 h, as monitored by the emergence of ^{1}H NMR signals of phenylacetic acid and *p*-aminobenzyl alcohol (Figures 3a; Supporting Information, Figure S21a). In contrast, no apparent **PP2** LCV degradation can be discerned in the absence of *PGA*. The generation of primary amine moieties (Figure S21b) was verified by amine-induced emission turn-on of fluorescamine (FA; Figure 3b). DLS measurements revealed that both $\langle D_h \rangle$ and scattering light intensities of **PP2** LCV dispersion decreased upon *PGA* digestion (Figure S22a,b). However, it was found that *PGA* cannot completely digest **PP2** LCVs into monomers even upon extended incubation, and *PGA*-treated LCVs dispersion exhibited an $\langle D_h \rangle$ of ≈100 nm when diluted into DMF (Figure S22c). The $\langle D_h \rangle$ measured in DMF is comparable to that in water (≈68 nm), and much larger than molecularly dissolved monomers. The morphology transition of vesicles was then monitored by TEM (Figure 3c). Upon *PGA* incubation for 4 h, coexistence of **PP2** LCVs with spherical nanoparticles were observed; at 12 h incubation, LCVs almost disappeared, accompanied with the emergence of nanoparticles and hollow nanostructures. After 24 h, only spherical nanoparticles were observed. Moreover, both TEM and AFM revealed the retention of spherical micelles when the final dispersion was diluted into DMF (Figures 3d; Supporting Information, Figure S22d). When *PGA*-treated **PP2** LCVs were dialyzed against water, lyophilized, and dispersed into D_2O, ^{1}H NMR analysis only revealed signals characteristic of PEG (Figure S21c). Taken together, we concluded that **PP2** LCVs transformed into core-crosslinked (CCL) spherical micelles upon *PGA* degradation.

Previous reports established that enzymatic degradation of polymeric assemblies can proceed by the monomer–aggregate exchange pathway;[5f] whereas in other cases the interior of polymeric assemblies is directly accessible to enzymes.[10] As for **PP2** LCVs, considering the relatively high CAC (critical aggregation concentration; Figure S11a and Table S3), *PGA* could digest monomer chains, which are in equilibrium with supramolecular aggregates in solution. Cascade reactions (cleavage of terminal groups, release of self-immolative linkers, and generation of primary amines) will shift the monomer-aggregate equilibrium and alter the hydrophilic/hydrophobic balance, resulting in the formation of spherical micelles (Figure S23). Enzymatically generated primary amines will undergo inter/intra-molecular amidation reactions, aided by suppressed amine pK_a owing to high local density and the relatively hydrophobic microenvironment. Intermolecular amidation reactions then lead to crosslinking

of nanoparticles. Enzymes may also directly digest into aggregates and in situ generate primary amines, followed by amidation-induced crosslinking (Figure S23). This crosslinking chemistry is quite comparable to our recent work concerning the fabrication cross-linked polymersomes under light irradiation.[8d] Furthermore, *PGA* and *Bla*-triggered transition from polymeric vesicles to CCL micelles for **PP4** and **PC1** were also confirmed by ^{1}H NMR, DLS, and TEM measurements (Figures 3e and S24,S25).

Microenvironmental polarity variation within polymeric vesicles during enzymatic degradation was explored. For 3-HF-labeled **PP6** LCVs, continuous increase of ESICT (451 nm) and decrease of ESIPT (537 nm) band intensities were observed when incubated with *PGA* (Figure S26), revealing a hydrophobic-to-hydrophilic transition of bilayers. This is reasonable considering that enzymatic uncapping and self-immolative rearrangement will remove hydrophobic side groups; newly generated amines will either be protonated or participate in amidation, and all of these reactions will endow CCL nanoparticle interiors with hydrophilicity.

Enzyme-triggered cargo release was then evaluated. CLSM and fluorescence analysis confirmed sustained release of calcein, NR, and tetramethylrhodamine-dextran from **PP2** LCVs mediated by *PGA* (Figures S27–S29). Moreover, initial enzyme concentrations considerably affect the rate of microenvironmental polarity switching and cargo release profiles (Figure S30). Next, *PGA*-triggered release of gentamicin (GEN), a hydrophilic aminoglycoside antibiotic, from **PP2** LCVs was tested against the highly opportunistic Gram-negative pathogen, *P. aeruginosa*. Neither **PP2** LCVs nor *PGA* exhibited appreciable growth inhibition of *P. aeruginosa* (Figure S31a,b). However, upon GEN loading and *PGA* actuation, **PP2** LCVs showed a prominent growth inhibition effect comparable to that of free GEN when the equivalent GEN concentration was higher than 1.0 μg mL^{-1}. In contrast, largely compromised antibacterial activity was observed without *PGA*, which can be ascribed to the poor permeability of hydrophilic guest molecules through intact **PP2** LCV bilayers (Figure 4a).

Methicillin-resistant *Staphylococcus aureus* (MRSA) poses a huge threat to public health, and one main cause of MRSA resistance is the production of *Bla*. Considering combination therapy is a clinically important treatment option for MRSA, a pair of semisynthetic streptogramin antibiotics, quinupristin/dalfopristin (Synercid), was concomitantly loaded into **PC1** vesicles to evaluate anti-MRSA activity (Figure 4b). Significantly, both free Synercid and **PC1** vesicles encapsulating Synercid efficiently inhibited MRSA growth. In contrast, MRSA strains continued to grow in the presence of *Bla*-inert **PS1** vesicles encapsulating Synercid at comparable equivalent drug concentrations.

In addition to enhanced stability, reduced side effects, and the feasibility of combination therapy, encapsulation of antibiotics into enzyme-responsive polymeric vesicles could also achieve resistant bacteria-selective drug delivery. To this end, vancomycin (VAN), a glycopeptide antibiotic for effectively treating MRSA infections, was encapsulated into **PC1** vesicles. After studying in vitro VAN release activated by *Bla* (Figure S27d), the anti-MRSA activity was examined. At

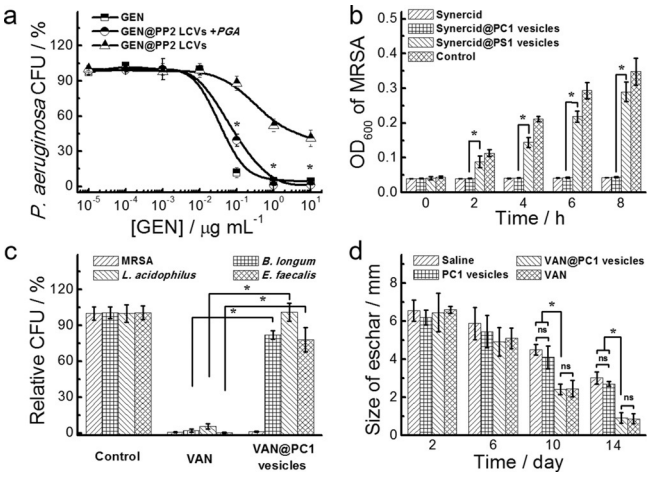

Figure 4. a) GEN-equivalent concentration dependent *P. aeruginosa* inhibition of GEN, GEN-loaded **PP2** LCVs in the absence and presence of *PGA*. b) Time-dependent MRSA growth inhibition of Synercid-loaded **PC1** vesicles. c) Growth inhibition effects of VAN and VAN-loaded **PC1** vesicles against MRSA, *B. longum*, *L. acidophilus*, and *E. faecalis*. d) Burn wound size analysis. ns, no statistically significant differences; $*p < 0.05$, student's *t*-test.

a drug concentration higher than 1.0 μg mL^{-1}, VAN-loaded **PC1** vesicles significantly inhibited MRSA growth, comparable to that of free VAN (Figure S32a). In contrast, *Bla*-inert **PS1** vesicles loaded with VAN cannot efficiently kill MRSA even at much higher drug concentrations. In control experiments, blank **PC1** and **PS1** vesicles exhibited negligible effect on MRSA growth (Figure S31c,d). The crucial role of *Bla* in regulating VAN release from **PC1** vesicles was further verified by the addition of metallo-*Bla* inhibitor, zinc ion chelator EDTA. Although both free VAN and VAN-loaded **PC1** vesicles prominently inhibited MRSA growth, the co-incubation with *Bla* inhibitor led to negligible inhibitory effects (Figure S32b).

We further examined MRSA-selective antibiotic release from **PC1** vesicles (Figure 4c). Free VAN can completely inhibit the growth of both probiotics (*B. longum*, *L. acidophilus*, and *E. faecalis*) and MRSA, which should be avoided under practical circumstances. Significantly, when co-incubated with VAN-loaded **PC1** vesicles at equivalent drug concentrations, only the MRSA strain was significantly inhibited. The selectivity should be ascribed to the fact that common probiotics cannot produce *Bla*, thus **PC1** vesicles encapsulating VAN exhibit no bioactivities.

Bacterial strain-selective delivery of antibiotics is highly advantageous for slowing the evolution of drug resistance and avoiding antibiotic abuse/misuse. For example, the combination of conventional antibiotics with enzyme-responsive vesicles loaded with new-generation drugs could be utilized, so that resistant strains can be killed by potent drugs released from vesicles by specific enzymes, whereas non-resistant strains could be eliminated by conventional ones. Enzyme-responsive polymeric vesicles loaded with antibiotics could also directly serve as wound healing enhancers (Figure S33). As a proof-of-concept, topical treatment of MRSA-infected burn wound with VAN-loaded **PC1** vesicles were conducted.

Note that blank **PC1** vesicles exhibited negligible effects on the growth of both mammalian and bacterial cells (Figure S34 and Table S4). In the in vivo murine infected burn wound model, enhanced wound healing process was observed when treated with VAN and VAN-loaded **PC1** vesicles, as compared to the control groups (Figures 4 d; Supporting Information, Figure S35).

In summary, *PGA* and *Bla*-responsive polymeric vesicles were fabricated and enzyme-mediated degradation processes and microstructural evolution were studied. Enhanced structural stability, reduced side effects, feasibility of combination therapy, bacterial strain-selective delivery of potent antibiotics, and enhanced burn wound healing were achieved on the basis of antibiotic-loaded responsive vesicles. Overall, the modular design of enzyme-responsive vesicles from amphiphilic block copolymers, sharing the same backbone scaffold attached with different types of enzymatic substrates in the side chain, opens up new avenues to construct next-generation antimicrobial systems with improved efficacy for combating against virulent resistant pathogens.

Acknowledgements

This work was supported by the National Natural Scientific Foundation of China (NNSFC) Projects (21274137 and 51033005) and Specialized Research Fund for the Doctoral Program of Higher Education (SRFDP, 20123402130010).

Keywords: antibiotic resistance · β-lactamase · block copolymers · enzyme-responsive · polymeric vesicles

How to cite: *Angew. Chem. Int. Ed.* **2016**, *55*, 1760 – 1764
Angew. Chem. **2016**, *128*, 1792 – 1796

[1] S. B. Levy, B. Marshall, *Nat. Med.* **2004**, *10*, S122 – S129.
[2] a) L. Zhang, D. Pornpattananangkul, C. M. J. Hu, C. M. Huang, *Curr. Med. Chem.* **2010**, *17*, 585 – 594; b) A. P. Blum, J. K. Kammeyer, A. M. Rush, C. E. Callmann, M. E. Hahn, N. C. Gianneschi, *J. Am. Chem. Soc.* **2015**, *137*, 2140 – 2154.
[3] a) K. Wayakanon, M. H. Thornhill, C. W. I. Douglas, A. L. Lewis, N. J. Warren, A. Pinnock, S. P. Armes, G. Battaglia, C. Murdoch, *FASEB J.* **2013**, *27*, 4455 – 4465; b) D. D. Lane, F. Y. Su, D. Y. Chiu, S. Srinivasan, J. T. Wilson, D. M. Ratner, P. S. Stayton, A. J. Convertine, *Polym. Chem.* **2015**, *6*, 1255 – 1266; c) K. T. Kim, J. J. L. M. Cornelissen, R. J. M. Nolte, J. C. M. van Hest, *Adv. Mater.* **2009**, *21*, 2787 – 2791; d) R. J. R. W. Peters, M. Marguet, S. Marais, M. W. Fraaije, J. C. M. van Hest, S. Lecommandoux, *Angew. Chem. Int. Ed.* **2014**, *53*, 146 – 150; *Angew. Chem.* **2014**, *126*, 150 – 154; e) D. Gräfe, J. Gaitzsch, D. Appelhans, B. Voit, *Nanoscale* **2014**, *6*, 10752 – 10761.
[4] a) S. Mura, J. Nicolas, P. Couvreur, *Nat. Mater.* **2013**, *12*, 991 – 1003; b) F. H. Meng, Z. Y. Zhong, J. Feijen, *Biomacromolecules* **2009**, *10*, 197 – 209; c) O. Onaca, R. Enea, D. W. Hughes, W. Meier, *Macromol. Biosci.* **2009**, *9*, 129 – 139; d) M. H. Li, P. Keller, *Soft Matter* **2009**, *5*, 927 – 937; e) E. R. Gillies, T. B. Jonsson, J. M. J. Frechet, *J. Am. Chem. Soc.* **2004**, *126*, 11936 – 11943; f) M. L. Viger, M. Grossman, N. Fomina, A. Almutairi, *Adv. Mater.* **2013**, *25*, 3733 – 3738; g) J. Thévenot, H. Oliveira, O. Sandre, S. Lecommandoux, *Chem. Soc. Rev.* **2013**, *42*, 7099 – 7116.
[5] a) C. Wang, Q. S. Chen, Z. Q. Wang, X. Zhang, *Angew. Chem. Int. Ed.* **2010**, *49*, 8612 – 8615; *Angew. Chem.* **2010**, *122*, 8794 – 8797; b) M. P. Chien, M. P. Thompson, C. V. Barback, T. H. Ku, D. J. Hall, N. C. Gianneschi, *Adv. Mater.* **2013**, *25*, 3599 – 3604; c) R. V. Ulijn, *J. Mater. Chem.* **2006**, *16*, 2217 – 2225; d) R. de la Rica, D. Aili, M. M. Stevens, *Adv. Drug Delivery Rev.* **2012**, *64*, 967 – 978; e) J. Y. Rao, C. Hottinger, A. Khan, *J. Am. Chem. Soc.* **2014**, *136*, 5872 – 5875; f) J. Guo, J. M. Zhuang, F. Wang, K. R. Raghupathi, S. Thayumanavan, *J. Am. Chem. Soc.* **2014**, *136*, 2220 – 2223; g) I. Rosenbaum, A. J. Harnoy, E. Tirosh, M. Buzhor, M. Segal, L. Frid, R. Shaharabani, R. Avinery, R. Beck, R. J. Amir, *J. Am. Chem. Soc.* **2015**, *137*, 2276 – 2284; h) R. J. Amir, S. Zhong, D. J. Pochan, C. J. Hawker, *J. Am. Chem. Soc.* **2009**, *131*, 13949 – 13951; i) J. M. Hu, G. Q. Zhang, S. Y. Liu, *Chem. Soc. Rev.* **2012**, *41*, 5933 – 5949.
[6] a) R. J. Holt, G. T. Stewart, *J. Gen. Microbiol.* **1964**, *36*, 203 – 213; b) K. Bush, G. A. Jacoby, A. A. Medeiros, *Antimicrob. Agents Chemother.* **1995**, *39*, 1211 – 1233.
[7] a) G. J. M. Habraken, M. Peeters, P. D. Thornton, C. E. Koning, A. Heise, *Biomacromolecules* **2011**, *12*, 3761 – 3769; b) P. S. Pramod, K. Takamura, S. Chaphekar, N. Balasubramanian, M. Jayakannan, *Biomacromolecules* **2012**, *13*, 3627 – 3640; c) A. R. Rodriguez, J. R. Kramer, T. J. Deming, *Biomacromolecules* **2013**, *14*, 3610 – 3614; d) D. Bacinello, E. Garanger, D. Taton, K. C. Tam, S. Lecommandoux, *Biomacromolecules* **2014**, *15*, 1882 – 1888; e) K. S. Tücking, S. Handschuh-Wang, H. Schonherr, *Aust. J. Chem.* **2014**, *67*, 578 – 584; f) S. Haas, N. Hain, M. Raoufi, S. Handschuh-Wang, T. Wang, X. Jiang, H. Schonherr, *Biomacromolecules* **2015**, *16*, 832 – 841; g) M. Wang, C. Zhou, J. Chen, Y. Xiao, J. Du, *Bioconjugate Chem.* **2015**, *26*, 725 – 734.
[8] a) P. L. Carl, P. K. Chakravarty, J. A. Katzenellenbogen, *J. Med. Chem.* **1981**, *24*, 479 – 480; b) A. Alouane, R. Labruère, T. Le Saux, F. Schmidt, L. Jullien, *Angew. Chem. Int. Ed.* **2015**, *54*, 7492 – 7509; *Angew. Chem.* **2015**, *127*, 7600 – 7619; c) A. Sagi, R. Weinstain, N. Karton, D. Shabat, *J. Am. Chem. Soc.* **2008**, *130*, 5434 – 5435; d) X. R. Wang, G. H. Liu, J. M. Hu, G. Y. Zhang, S. Y. Liu, *Angew. Chem. Int. Ed.* **2014**, *53*, 3138 – 3142; *Angew. Chem.* **2014**, *126*, 3202 – 3206.
[9] a) Y. Y. Mai, A. Eisenberg, *Chem. Soc. Rev.* **2012**, *41*, 5969 – 5985; b) A. Blanazs, S. P. Armes, A. J. Ryan, *Macromol. Rapid Commun.* **2009**, *30*, 267 – 277.
[10] S. Samarajeewa, R. Shrestha, Y. L. Li, K. L. Wooley, *J. Am. Chem. Soc.* **2012**, *134*, 1235 – 1242.

Received: October 8, 2015
Revised: November 16, 2015
Published online: December 22, 2015

